A Model of the Ethylene Signaling Pathway and its Gene Response in *Arabidopsis thaliana*: Noise-Filtering Properties

José Diaz
Elena R. Alvarez-Buylla

SFI WORKING PAPER: 2006-03-009

SANTA FE INSTITUTE

A model of the ethylene signaling pathway and its gene response in *Arabidopsis thaliana*: noise-filtering properties

José Díaz[+] and Elena R. Álvarez-Buylla[+, ++]

[+]*Laboratorio de Genética, Desarrollo y Evolución de Plantas. Departamento de Ecologia Funcional. Instituto de Ecologia, UNAM, CU., Mexico D.F. 04510, Mexico*

[++] ***To whom correspondence should be addressed at:*** *Laboratorio de Genetica, Desarrollo y Evolucion de Plantas. Departamento de Ecologia Funcional. Instituto de Ecologia, Universidad Nacional Autónoma de México, Ciudad Universitaria., Mexico Distrito Federal. 04510, Mexico. E-mail: ealvarez@miranda.ecologia.unam.mx*

Abstract
Dynamic models of molecular networks and pathways enable *in silico* evaluations of the consistency of proposed interactions and the outcomes of perturbations as well as of hypotheses on system-level structure and function. We postulate a continuous model of the activation dynamics of the ETHYLENE RESPONSE FACTOR 1 (***ERF1***) gene in response to ethylene signaling. This activation elicits the response of the PLANT DEFENSIN 1 (***PDF1***) gene, which also responds to jasmonic acid, and the inhibition of the PUTATIVE AUXIN RESPONSIVE FACTOR 2 (***ARF2***) gene, that also responds to auxin. Our model allows the effect of different ethylene concentrations in eliciting contrasting genetic and phenotypic responses to be evaluated and seems to consider key components of the ethylene pathway because the ***ERF1*** dose-response curve that we predict has the same qualitative form as the phenotypic dose-response curves obtained experimentally. Therefore, our model suggests that the phenotypic dose-response curves obtained experimentally could be due, at least in part, to ERF1 changes to different ethylene concentrations. Stability analyses show that the model's results are robust to parameter estimates. Of interest is that our model predicts that the ethylene pathway may filter stochastic and rapid chaotic fluctuations in ethylene availability. This novel approach may be applied to any cellular signaling and response pathway in plants and animals.

Running title:
Arabidopsis ethylene signaling system; ethylene pathway cross-talk; ethylene pathway noise filtering properties.

Hormones are key signaling molecules for animal and plant cell function and they generally have non-linear responses to environmental factors. Also, different hormone pathways are not independent from each other. Non-linear dynamic models are thus necessary tools for understanding how living cells integrate and respond to various hormone pathways that imply the concerted action of multiple genes and molecules. As data on the plant experimental system, *Arabidopsis thaliana,* accumulate testable models to study the dynamic behavior of hormone signaling and response pathways are becoming possible and necessary. In this paper we present a model that simulates the activation response of a gene array involved in the *A. thaliana* ethylene signaling and response pathway in the face of different concentrations and temporal regimes of this key plant hormone. This model is grounded on available experimental data for the ethylene pathway, and enables *in silico* evaluations of the consistency of proposed interactions and the outcomes of perturbations, as well as novel hypotheses for this system behavior. The response genes considered are also targets of pathways of other important plant hormones (jasmonic acid and auxin) and thus provides a first approximation to studying how hormone pathways are interconnected via shared nodes and provides a novel mechanistic explanation for some observed phenotypes. Our model recovers observed results and it is used also to propose novel hypotheses that can be tested experimentally. Interestingly, our model predicts that the ethylene pathway may filter stochastic and rapid chaotic fluctuations in ethylene availability. The approach proposed here may be adapted to other cellular signaling and response pathway in plants and animals.

Introduction

Understanding the behavior of complex and integrated biological systems and the consequences of intervening in them present serious challenges to contemporary biologists. One of the requirements to meeting these challenges is the development and application of dynamic models. Boolean or discrete network models which focus on the nonlinear interactions between functions of gene expression or the activity of their products, but consider variables, functions and parameters that can take a limited number of integral values (0 and 1 in the simple Boolean case), have been used for modeling complex regulatory networks of cell or segment identities in animals and plants. Recent studies support their suitability and suggest that it is the topology of these complex networks and not the precise form of the kinetic functions of gene activities and interactions which underlies developmental identities in a predictable and robust manner and that such robustness has important functional and evolutionary significance (Mendoza, L. & Alvarez-Buylla, 2000; Von Dassow, Meir, Munro & Odell, 2000; Albert & Othmer, 2003; Espinosa-Soto, Padilla-Longoria & Alvarez-Buylla, 2004; Perkins, Hallett & Glass, 2004).

In contrast, Boolean or discrete modeling might be limited to address important aspects of the cellular mechanisms of signal perception and response. In this paper we use a continuous model to analyze the dynamic behavior of genes that are common targets of different hormone pathways in response to different concentrations of ethylene that is an important phytohormone. The model presented here is a useful tool to further our understanding of the interconnections among signaling pathways via common nodes and the long-held observation that different concentrations of the same hormone yield contrasting gene expression and phenotypic effects.

We also explore the consequences of different temporal regimes of a signal on genetic responses within a cell.

Signal transduction pathways are complex and dynamic systems by which biological cells perceive and respond to environmental and internal cues. However, to date, no theoretical model has linked the intensity and temporal regime of the external signal that triggers a particular signal transduction pathway to the activation of specific genes that may be the key in orchestrating cellular responses and integrating several response pathways to the original signal.

In the model plant *Arabidopsis thaliana*, an important signaling pathway in response to ethylene, a gaseous plant-specific growth regulator hormone, is implicated in the triple response of etiolated seedlings (Kieber, 1997; Chang. & Stadler, 2001; Chang, 2003; Guo & Ecke, 2004) and in several key aspects of plant development such as seed germination, cell elongation, fruit ripening, and organ senescence and abscission (for recent reviews: Guo & Ecke, 2004; Stepanova & Alonso, 2005). The pleiotropic effects of phytohormones and the fact that genetic and phenotypic effects of plant hormones are concentration-dependent have made functional analyses of plant hormones very complicated. In addition, recent experimental evidence suggests that all or most hormone pathways are interconnected in complex ways.

In this paper we use the ethylene signaling pathway to exemplify an approach that links signaling regimes and cellular genetic responses. Ethylene is the smallest of the phytohormones and we propose a specific dynamic continuous model for a single-cell response pathway to ethylene in *Arabidopsis* roots. We explicitly consider the probability that specific genes are activated or inactivated in response to different concentrations and temporal regimes of ethylene signaling. We explicitly evaluate the effects of varying concentrations of ethylene on the probability of activating ETHYLENE RESPONSE FACTOR 1 (*ERF1*), which could, in turn, activate genes like PLANT DEFENSIN 1 (*PDF1*), part of the jasmonate acid pathway (Ton et al., 2002; Brown et al., 2003) or inhibit genes like the PUTATIVE AUXIN RESPONSIVE FACTOR 2 (*ARF2*) (Lorenzo et al., 2003; Li et al., 2004) which responds to auxin. The model could provide a possible explanation for the experimental dose-response curves obtained in Chen & Bleecker (1995). Our model predicts that the phenotypic response curves obtained by these authors for mutants of upstream signaling components could be due, at least in part, to ERF1 changes to different ethylene concentrations. In fact, the ***ERF1*** dose-response curve that we predict has the same qualitative form as the phenotypic dose-response curves obtained by Chen & Bleecker (1995), and is robust to parameter fluctuations. It also shows that the response of the three-gene array yields a continuous probability distribution for the activation states of the three genes for any given ethylene concentration. This probability distribution may be interpreted as the plastic responses of *Arabidopsis* root cells to the environmental factors that trigger ethylene signaling and response. Dynamic mechanisms that underlie plastic cellular responses may be particularly important in plants that are sessile and rely on plastic developmental and growth responses to contend with changing environmental conditions.

We also simulated different temporal regimes of ethylene signaling and found that gene expression fluctuated when ethylene signaling was simulated as an ordered periodic temporal pattern. However, when a chaotic temporal ethylene signaling pattern was assumed, the probability of activation of the three genes fluctuated and tended to a chaotic attractor only when

the fluctuations were slow, suggesting that the system is unable to respond to input signals that fluctuate very rapidly. Stochastic ethylene fluctuations were only reflected in stochastic expression fluctuations of the gene directly affected by ethylene (***ERF1***), suggesting that the cell translational machinery may filter out stochastic fluctuations. The novel predictions of this study may extend to other signaling and response pathways in both plants and animals.

Model for the ethylene response

Two antagonist modules have been documented for the ethylene signaling and response pathway (Guo & Ecke, 2004; Fig. 1). In the first, inside the endoplasmic reticulum (ER), a MAPK module, in which the MAPKKK molecule is the constitutive triple response 1 (CTR1) molecule (a Raf-like serine/threonine kinase (Guo & Ecke, 2004)), is constitutively active when either one of the ethylene receptors is active; this causes EIN2 (*ETHYLENE INSENSITIVE 2*) molecule to be inactive (Bleecker et al., 1998). In the second, a module in the nucleus membrane is activated when ethylene binds to its receptors. In the latter case, EIN2 is activated, thereby allowing activation of the EIN3 transcription factor, which then binds to the ***ERF1*** promoter (Guo & Ecke, 2004). ERF1 binds to GCC boxes located in the promoter regions of various genes, such as ***PDF1***. Also, ethylene negatively regulates **ARF2** protein accumulation in a ***HOOKLESS1*** dependent manner (Lorenzo et al., 2003; Li et al., 2004; Guo & Ecker, 2004).

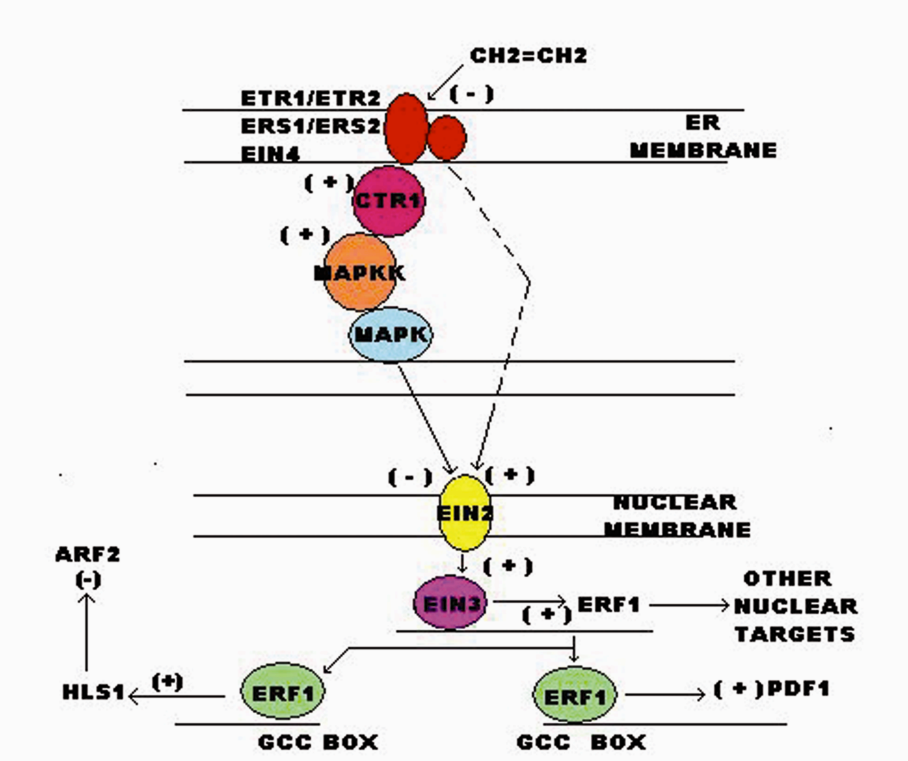

Fig. 1. The ethylene pathway consists of two antagonist modules. The first consists of a MAPK module that is constitutively activated when either one of the ethylene receptor types is constitutively active. When the MAPK module is activated, the EIN2 molecule is inactive. The second module is located in the cell nucleus and is activated when the ethylene molecule binds to its receptor. In this case, the EIN2 molecule is activated, thereby allowing the subsequent activation of the EIN3 transcription factor, which binds to the ***ERF1*** promoter. In the final step, the ERF1 transcription factor binds to GCC boxes located in the promoter regions of various genes, such as ***PDF1***, and inhibits genes like ***ARF2***, subsequently producing the ethylene response in the plant root. The dashed arrow only indicates the positive effect of the inhibition of the ethylene receptor on the activation of EIN2 and not a direct mechanism of activation.

We use ordinary differential equations and two-state Markov chains to model: (1) the activation dynamics of ***ERF1*** in response to ethylene signaling, which in turn elicits the response of ***PDF1*** that also responds to jasmonic acid, and (2) the ***HLS1***-dependent inhibition of ***ARF2***, a gene that also responds to auxin. The activation of ***PDF1*** induces the transcription of a defensin, protein which is also part of the jasmonate-dependent defense response (Ton et al., 2002; Brown et al., 2003), while ***ARF2*** regulates the activity of the auxin signaling pathway and is involved in the light-dependent seedling apical hook development. Exposure to light decreases HLS1 protein levels and evokes a concomitant increase in ARF2 accumulation (Li et al., 2004).

We present a detailed derivation of the mathematical model of the ethylene response in the Appendix I of this manuscript, and a summary of the equations, initial conditions and parameter values are presented in Table 1 shown below. The equations were numerically integrated using the predictor-corrector Euler method with a fixed time step of 0.04s. We present the stability analysis of the model in the Appendix 2 of the manuscript.

Table 1. One-cell ethylene model: differential equations and parameters (ET is given in μM).

1. Equations for the inactivation of the ethylene receptor:

$$\frac{dETR^{(-)}}{dt} = \kappa_1 (ET - ETR^{(-)})\left(ETR_T - ETR^{(-)}\right) - \kappa_2 ETR^{(-)}$$

$$ETR_T = ETR^{(+)} + ETR^{(-)}$$

2. Equations for the CTR1 module:

$$\frac{dCTR1^*}{dt} = \kappa_3 \left(ETR_T - ETR^{(-)}\right)\left(CTR1_T - CTR1^*\right) - \kappa_4 CTR1^*$$

$$\frac{dMAPKK^*}{dt} = \kappa_5 CTR1^*\left(MAPKK_T - MAPKK^*\right) - \kappa_6 MAPKK^*$$

$$\frac{dMAPK^*}{dt} = \kappa_7 MAPKK^*\left(MAPK_T - MAPK^*\right) - \kappa_8 MAPK^*$$

3. Equations for the EIN2 module:

$$\frac{dEIN2^{(-)}}{dt} = \kappa_9 MAPKc^*\left(EIN2_T - EIN2^{(-)}\right) - \kappa_{10} EIN2^{(-)} \frac{ETR^{(-)}}{ETR^{(-)} + \beta}$$

$$EIN2_T = EIN2^{(+)} + EIN2^{(-)}$$

$$\frac{dEIN2^{(+)}}{dt} = -\frac{dEIN2^{(-)}}{dt}$$

$$\frac{dEIN3^*}{dt} = \kappa_{11} EIN2^{(+)}\left(EIN3_T - EIN3^*\right) - \kappa_{12} E1N3^*$$

$$\frac{dmRNA}{dt} = \frac{p^{on}(t) V_{trans} mRNA}{mRNA + \kappa_{15}} - \kappa_{16} mRNA$$

$$\frac{dERF1}{dt}\Big|_{ER} = \kappa_{17} mRNA - D_{erf1} ERF1$$

$$\frac{dERF1}{dt}\Big|_{nucleus} = D_{erf1} ERF1n - \kappa_{18} ERF1n$$

4. Equations for the activation of ERF1, PDF1 and ARF2 genes:

$$\frac{dp^{off}_{ERF1}}{dt} = -\kappa_{13} N_{ein3} p^{off}_{ERF1} + \kappa_{14} p^{on}_{ERF1}$$

$$\frac{dp^{on}_{ERF1}}{dt} = \kappa_{13} N_{ein3} p^{off}_{ERF1} - \kappa_{14} p^{on}_{ERF1}$$

$$N_{ein3} = 602.3 V_{nucleus} EIN3^*$$

$$\frac{dp^{on}_{PDF1}(t)}{dt} = \kappa_{19} N_{ERF1n} p^{off}_{PDF1}(t) - \kappa_{20} p^{on}_{PDF1}(t)$$

$$\frac{dp^{off}_{PDF1}(t)}{dt} = -\kappa_{19} N_{ERF1n} p^{off}_{PDF1}(t) + \kappa_{20} p^{on}_{PDF1}(t)$$

$$\frac{dp^{on}_{HLS1}(t)}{dt} = \kappa_{21} N_{ERF1n} p^{off}_{HLS1}(t) - \kappa_{22} p^{on}_{HLS1}(t)$$

$$\frac{dp^{off}_{HLS1}(t)}{dt} = -\kappa_{21} N_{ERF1n} p^{off}_{HLS1}(t) + \kappa_{22} p^{on}_{HLS1}(t)$$

Table 1. One-cell ethylene model: differential equations and parameters (ET is given in μM). (Continued)

5.- Adjust of MAPK concentration from ER to nucleus: $n_{MAPK} = 5x10^{-21}\, MAPK^*$ $MAPKc^* = 1.908x10^{18}\, n_{MAPK}$ **Adjustment of ERF1 concentration from ER to nucleus:** $n_{erf1} = 5x10^{-21}\, ERF1$ $ERF1n = 1.908x10^{18}\, n_{erf1}$	**6.- Initial conditions:** $CTR1^*(0) = 0.3\mu M$ $\quad ERF1(0) = 0;$ $ETR^{(-)}(0) = 0$ $\quad ERF1n(0) = 0;$ $MAPKK^*(0) = 0.5\mu M;$ $\quad p^{off}_{PDF1}(0) = 1;$ $MAPK^*(0) = 0.5\mu M;$ $\quad p^{on}_{PDF1}(0) = 0;$ $EIN2^{(-)}(0) = 0.005\mu M;$ $\quad p^{off}_{HLS1}(0) = 1;$ $EIN3^*(0) = 0;$ $p^{on}_{ERF1}(0) = 0;$ $p^{off}_{ERF1}(0) = 1;$
7. Parameter values: $\kappa_1 = 5\mu M^{-1}s^{-1}$; $\kappa_2 = 0.0003s^{-1}$; $\kappa_3 = 3\mu M^{-1}\, s^{-1}$; $\kappa_4 = 0.085s^{-1}$; $\kappa_5 = 9.196\mu M^{-1}\, s^{-1}$; $\kappa_6 = 4.598s^{-1}$; $\kappa_7 = 0.318\mu M^{-1}s^{-1}$; $\kappa_8 = 0.0954s^{-1}$; $\kappa_9 = 2\mu M^{-1}s^{-1}$; $\kappa_{10} = 0.005s^{-1}$; $\kappa_{11} = 5\mu M^{-1}s^{-1}$; $\kappa_{12} = 0.005s^{-1}$; $\kappa_{13} = 0.003s^{-1}$; $\kappa_{14} = 0.09s^{-1}$; $\kappa_{15} = 0.0001\mu M$; $\kappa_{16} = 0.0009s^{-1}$; $\kappa_{17} = 0.1972s^{-1}$; $\kappa_{18} = 0.198s^{-1}$; $\kappa_{19} = 0.0025s^{-1}$; $\kappa_{20} = 0.61s^{-1}$; $\kappa_{21} = 0.003s^{-1}$; $\kappa_{22} = 0.65s^{-1}$; _ = 6μM; $V_{trans} = 0.000003\mu Ms^{-1}$; $D_{erf1} = 0.99s^{-1}$; $ETR_T = 0.3\mu M$; $CTR1_T = 0.3\mu M$; $MAPKK_T = 0.5\mu M$; $MAPK_T = 0.5\ \mu M$; $EIN2_T = 0.005\mu M$; $EIN3_T = 0.005\mu M$; $V_{nucleus} = 524\mu m^3$.	**8. Variables:** ***ETR*** = concentration of ethylene receptor in cell membrane; ***ET*** = total concentration of ethylene outside the cell (**control variable**); ***CTR1**** = concentration of activated constitutive triple response1 protein; $MAPKK^*$ = concentration of activated mitogen-activated protein kinase kinase; $MAPK^*$ = concentration of activated mitogen-activated protein kinase; ***EIN2*** = concentration of ethylene insensitive 2 protein; ***EIN3**** = concentration of activated ethylene insensitive 2 protein; ***mRNA*** = concentration of messenger RNA in nucleus; ***ERF1*** = concentration of ERF1 transcription factor; N_{ein3} = number of activated EIN3 molecules in nucleus; N_{erf1} = number of activated ERF1 molecules in nucleus; $V_{nucleus}$ = nuclear volume; n_{MAPK} = number of moles of activated MAPK; $MAPKc^*$ = concentration of MAPK in nucleus; n_{erf1} = number of moles of activated ERF1 molecules; ***ERF1n*** = concentration of activated ERF1 transcription factor in nucleus. The symbol **(+)** means the activated form of the corresponding receptor, while the symbol **(-)** represents its inactivated form. The subscript ***T*** stands for the total concentration of the corresponding molecule.

Results

Probability of *ERF1*, *PDF1* and *ARF2* activation as a function of ethylene concentration.

In the ground state of a root cell in the absence of ethylene both ETR receptors are activated. In our model (Appendix I: Eqn. [2] of Model; Section 1 of Table 1), this state corresponds to $ETR^{(-)} = 0$ and $ETR^{(+)} = ETR_T = 0.3\mu M$. For this concentration of activated ETR, the system reaches, following a brief transient period, a steady state in which $CTR1 = 0.28\mu M$, $MAPKK = 0.18\mu M$ and $MAPK = 0.19\mu M$ (Appendix I: Eqns. [3], [4] and [5] of Model; Section 2 of Table 1). This set of values for the MAPK cascade represents the ground state in which the system remains steady in the absence of ethylene (Chang, 2003; Guo & Ecke, 2004).

Conversely, in the presence of ethylene, our model predicts that there is a threshold value of ethylene concentration above which the cascade is completely inactivated (Fig. 2, obtained from the numerical solution of Eqns. [3], [4] and [5] of Model in Appendix I and section 2 of

Table 1). This value is ~1μL/L, and above this value the activity of the cascade in the ER falls with increasing ethylene concentration. Thus, ethylene produces its effects even when the MAPK cascade has not been completely inactivated. The inactivation of the cascade strongly depends on the dynamical behavior of the ETR-CTR1 complex, as shown in figure 2*B*, in which we repeated the above calculations in the absence of the MAPKK and MAPK components of the kinase cascade, whose presence in the chain of reactions inside the ER has been put into doubt (Stepanova & Alonso, 2005). In this case, neither the threshold for inactivation nor its dependence on ethylene concentration is different to the ones found in cases in which the MAPKK and MAPK components were considered.

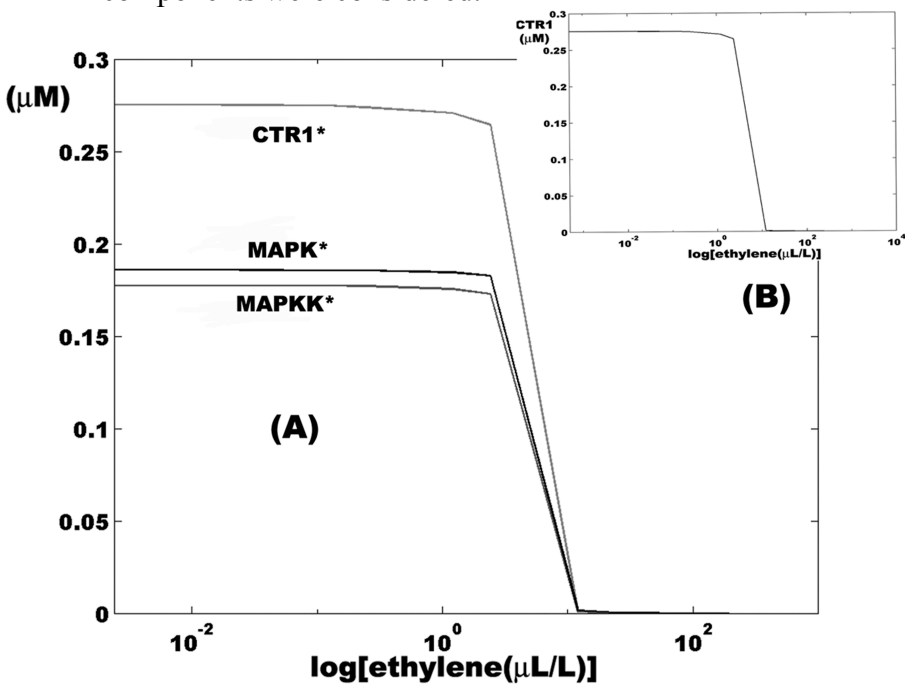

Fig. 2. *(A)* Inactivation of the MAPK cascade by ethylene. The curve shows a threshold value of ethylene concentration (~ 1μL/L) for the total inactivation of the cascade. Before this threshold value is reached, the concentration of activated CTR1, MAPKK and MAPK slowly decreases, indicating that there is a range of ethylene concentrations for which the root cells may exhibit a simultaneous activity of the MAPK cascade and the ethylene response molecular machinery. *(B)* Inactivation of CTR1 by ethylene in absence of MAPKK and MAPK. This curve shows a threshold value of ~ 1μL/L for the total inactivation of the kinase. This result indicates that the kinases downstream CTR1 are required only to ensure the fidelity of the signal transmitted to EIN2.

In Fig. 3A we show how the probability that ***ERF1*** is activated ("*on*" state), denoted by p^{on}_{ERF1}, changes as the concentration of ethylene increases, which is the first novel prediction emerging from our model (calculated from the numerical solution of Eqn. [10] of the Model in the Appendix I; see also Section 4 of Table1): *the probability that **ERF1** is activated as a function of the concentration of ethylene slowly increases following a sigmoid curve*.

This conclusion is unaffected by removing the equations for the MAPKK and MAPK activation from the set of equations of the model (see Section 2 of Table 1). In Fig. 3*B* we show the probability of activation of the ***ERF1*** gene as a function of ethylene concentration, without the incorporation of the two kinases. As is clearly observed the curve practically has no variations with respect to curve 3*A*, indicating that the above conclusion is independent of the form in

which the activation of the EIN2 molecules is controlled: directly by CTR1 in a one-step process or by a three-step process which includes the MAPKK and MAPK molecules.

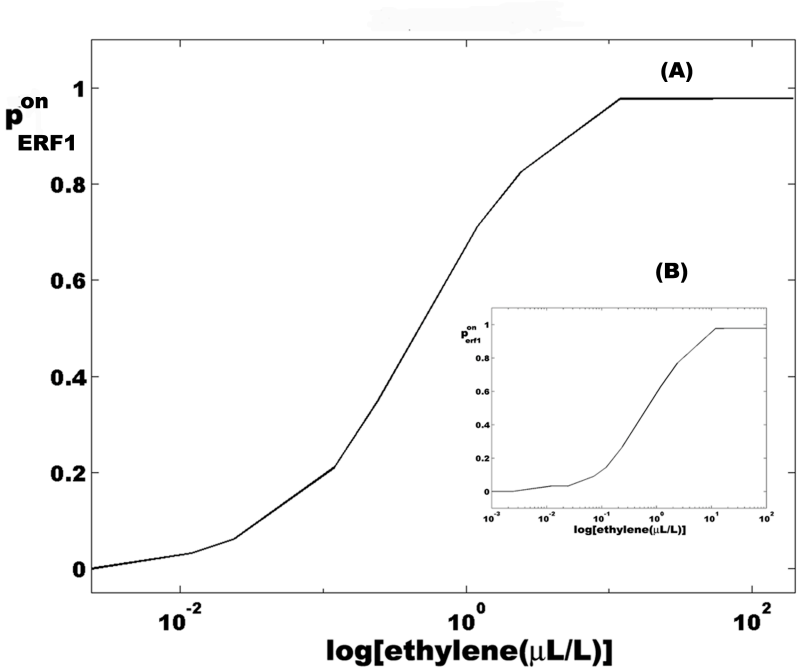

Fig. 3. *(A)* Dose-response curve for ***ERF1*** as a function of ethylene concentration. *(B)* Dose-response curve for ***ERF1*** as a function of ethylene concentration in the absence of MAPKK and MAPK in the chain of reactions of the model.

Thus, the model presented here provides testable hypotheses on how environmental perturbations perceived by a root cell via changes in ethylene concentrations affect the activation response of specific genes.

We may adjust the obtained dose-response curve predicted by our theoretical model to a Hill function as follows:

$$p_{ERF1}^{on} = \frac{0.9924 ET^{0.97}}{ET^{0.97} + 0.46} \quad \text{with a } R^2 = 0.9942 \qquad \text{[M.1]}$$

in which the Hill coefficient is 0.97 ± 0.029. This range contains the value of 0.99 reported by Chen and Bleecker (1995) for the experimentally documented dose-response curve of the wild-type *Arabidopsis* root to ethylene and strongly suggests that the assumptions made in the model for both parameters and functions capture important key aspects of the actual system operating inside plant cells. A Hill coefficient of approximately 1 indicates that it would not be adequate to model the activation kinetics of ***ERF1*** with a Boolean function because there is a wide range of ethylene concentrations values - from 0.01μL/L to 10μL/L - for which the probability of the state *on* of the gene takes values that are less than 1 but not close enough to zero to postulate an "all" or "none" response (Figs. 3*A* and 3*B*).

Equation [M.1] of main text (see above) also indicates that the genetic machinery of ethylene response is switched on even when the MAPK cascade is still in its activated state. Thus, for a wide range of ethylene concentrations, *Arabidopsis* cells should have a mix of states induced by both signaling pathways. In Figure A1 of the Appendix I (Model section), we show this in the phase portrait generated by the plot of activated *CTR1** vs. p^{on}_{ERF1}.

According to Eqns. [10], [12] and [13] of the Model presented in the Appendix I, once can be tabulated for each ethylene concentration, we can calculate the amount of ERF1 protein that can be produced in the ER in terms of , which determines the translation rate of ***ERF1*** in the following form:

$$v(t) = p^{on}_{ERF1}(t) V_{trans} \qquad [M.2]$$

where V_{trans} is the maximum rate of translation of the gene (Section 7 of Table 1 and Eqn. [12] of Model in Appendix I), assuming that the overall rate of translation of ***ERF1*** can be modeled with a Michaelis-Menten type of equation.

In Fig. 4 we show the amount of ERF1 protein that accumulates in the nucleus as a function of the ethylene concentration. As observed in this figure, the model can also be used to predict the *concentration of ERF1 protein accumulated in the nucleus as a function of the ethylene concentration* and this could, in principle, be tested experimentally.

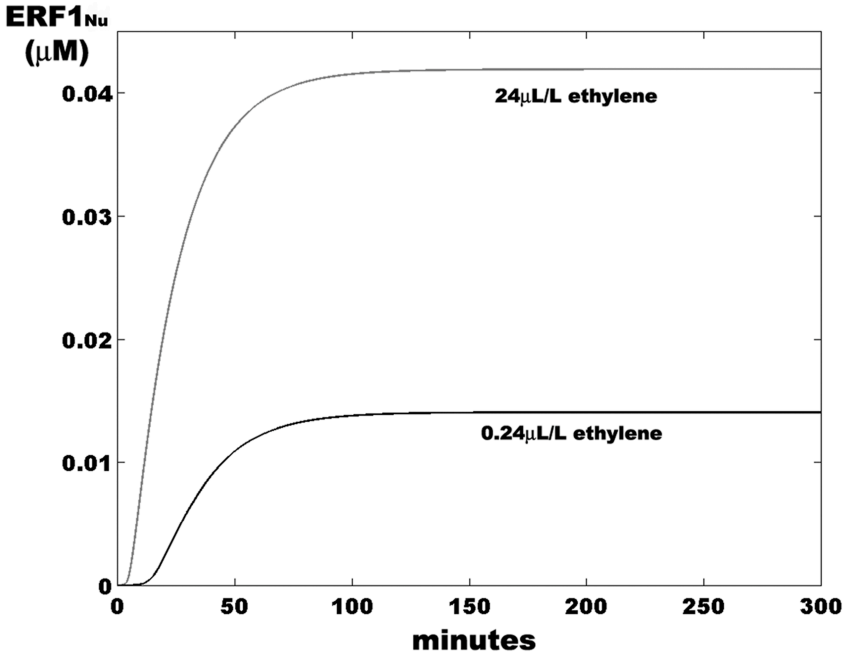

Fig. 4. Amount of ERF1 protein accumulated in the nucleus for two different concentrations of ethylene. As the concentration of the phytohormone is increased the rate and amount of ERF1 accumulation is also increased.

According to the experimental evidence, ERF1 continuously moves from the ER into the nucleus (by some yet uncharacterized mechanism), activating a series of genes - *for example*,

PDF1 - and inactivating others, such as ***ARF2***. From the value of the nuclear concentration of the ERF1 protein (Section 5 of Table 1 and Fig. 4) it is possible to calculate the respective number of ERF1 molecules in the nucleus (Section 4 of Table 1). With this value, Eqns. [15] and [16] of the Model (Section 4 of Table 1 see also Appendix I) can be used to obtain the probabilities that the ***PDF1*** and ***ARF2*** genes are active (in the *"on*" state) as a function of *ethylene concentration*. Therefore, we can summarize the state of the three genes by a point ($p^{on}_{ERF1}, p^{on}_{PDF1}, p^{on}_{ARF2}$) in a three-dimensional probability space, in which each point represents the activity configuration of the array for each ethylene concentration. The succession of the values of ($p^{on}_{ERF1}, p^{on}_{PDF1}, p^{on}_{ARF2}$) constitutes the trajectory of the gene array in this probability space. In Fig. 5, we show three possible steady-state configurations of the array for three different concentrations of ethylene.

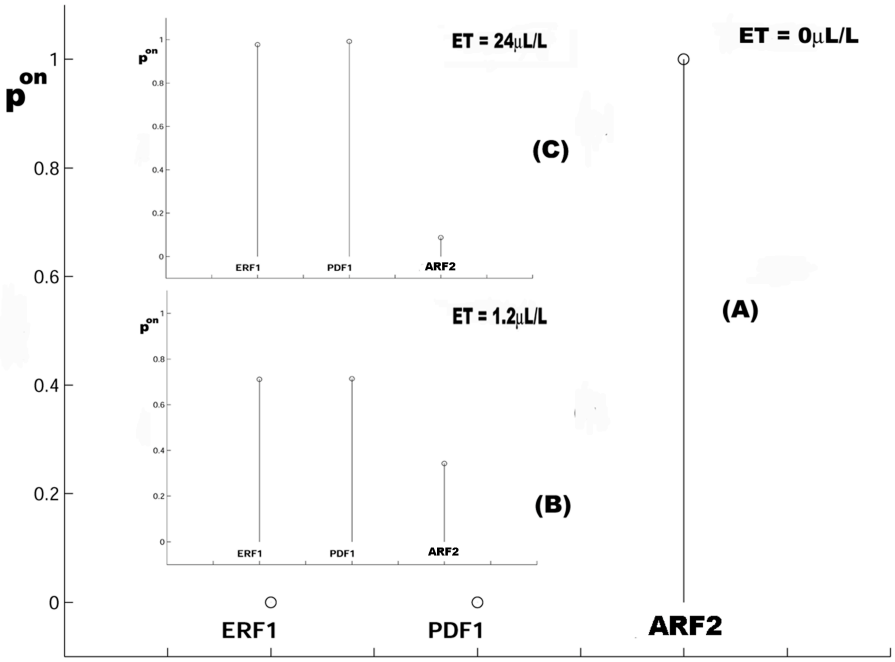

Fig. 5. (*A*) Steady-state activity configuration of the array conformed by the ***ERF1***, ***PDF1*** and ***AXR2*** genes in the absence of ethylene. This configuration corresponds to the point (0, 0, 1) in the probability space for the array. (*B*) Activity configuration of the array in the presence of less than 0.24μL/L ethylene. This configuration corresponds to the point (0.35, 0.58, 0.50) in the probability space for the array. (*C*) Activity configuration of the array in the presence of less than 24μL/L of ethylene. This configuration corresponds to the point (0.98, 0.80, 0) in the probability space for the array.

Filtering properties of the ethylene response system

A dynamic and continuous system such as the one proposed here for simulating a specific signaling and response pathway (to a hormone in this case) enables us to predict the temporal patterns of gene response to different temporal regimes of ethylene signaling. Such predictions can be tested experimentally. We specifically set out to analyze the behavior of the three-gene array considered in our system in response to different ethylene signaling regimes. The first step was to study the dynamical response of the three-gene array to an ordered pattern of periodic

variations in ethylene concentration. In order to characterize this kind of response, we used the sinusoidal signal $ET(t) = 0.5 + 0.5\sin(\omega t)$, where *ET* is the ethylene concentration. The response of the ***ERF1*** gene to this function is shown in Fig. 6*A*. It is clear from the figure that p^{on}_{ERF1} also becomes periodic, showing a maximum and a minimum value for each value of ω. In every case, the maximum probability for the *on* state of the gene is practically unaffected by the periodic variations in the input signal. However, the minimum probability value is clearly affected, giving rise to oscillations of p^{on}_{ERF1} with a small amplitude for $\omega < 0.00001 s^{-1}$ and $\omega > 0.001 s^{-1}$ and with a larger amplitude in the interval between these values. As we have $\omega = 2\pi / T$, where *T* is the period of the signal, the maximum response of the ***ERF1*** gene to *ET(t)* increases in the interval of *T* values between 0.35h (~20min) and 174h ($0.00001 s^{-1} < \omega < 0.005 s^{-1}$). Figure 6*B* shows the trajectory of the three-gene system in the probability space for the array that falls under the fluctuations in ethylene concentration given by the function *ET(t)* with $\omega = 0.00005 s^{-1}$. This graph shows the trajectory of the array towards a cycle following a transient response to the input.

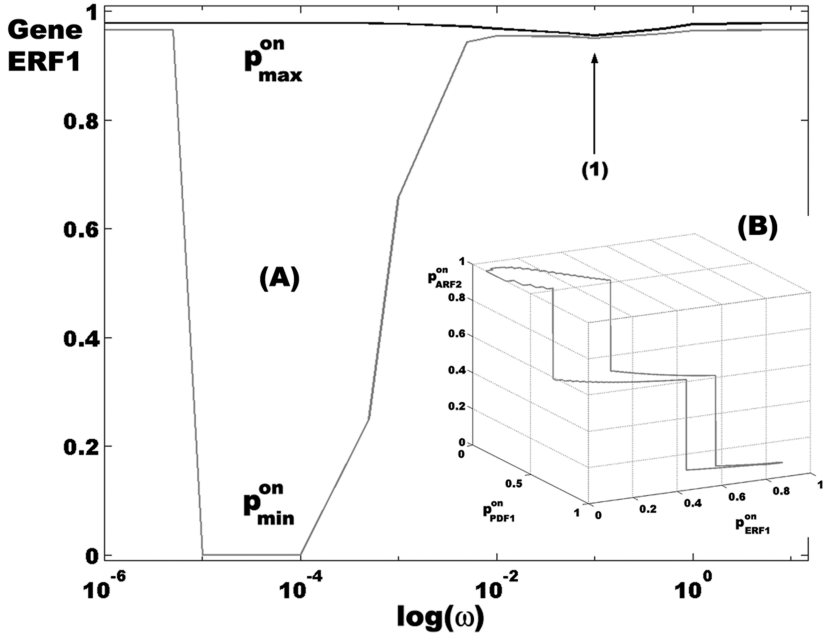

Fig. 6. (*A*) Values of $p^{on}_{\max}$ and $p^{on}_{\min}$ for the ***ERF1*** gene as a function of the angular frequency of function *ET(t)*; the number (1) indicates the minimum value of the response of ***ERF1***. (*B*) Cyclic response of the three-gene array to the periodic changing environmental conditions simulated by the function *E(t)*.

If the model proposed here does indeed capture the key elements of the dynamic genetic response of *Arabidopsis* cells to ethylene signaling elicited by changing internal or external cues, then such a cycle can simulate the type of continuous genetic adjustments that may occur inside *Arabidopsis* cells in response to periodic ordered environmental fluctuations. In turn, such genetic responses may underlie the visible periodic changes in the plant following physiological or even plastic morphological adjustments.

These results lead to the question of how the system responds when the environmental conditions consist of stochastic fluctuations. To simulate this situation, we represented the input signal by non-Gaussian stochastic fluctuations in ethylene concentration between 0μM and 1μM (24μL/L), with the ethylene concentration changing every 360s. As we show in Fig. 7, the random fluctuations are reflected in the p^{on}_{ERF1} value but are practically absent in the probability of the *on* state of the remaining genes. This results in the trajectory of the system in the probability space being a smooth curve that leads the system to a probability subspace in which the state of the system changes randomly as a consequence of the random changes in p^{on}_{ERF1} (Fig. 7). Thus, the fluctuating environmental conditions are reflected only in the activation of the gene directly affected by ethylene (***ERF1***), and they apparently do not affect the expression of the genes downstream of ***ERF1***, indicating that the cell translation machinery filters any possible fluctuation in the level of mRNA from this gene.

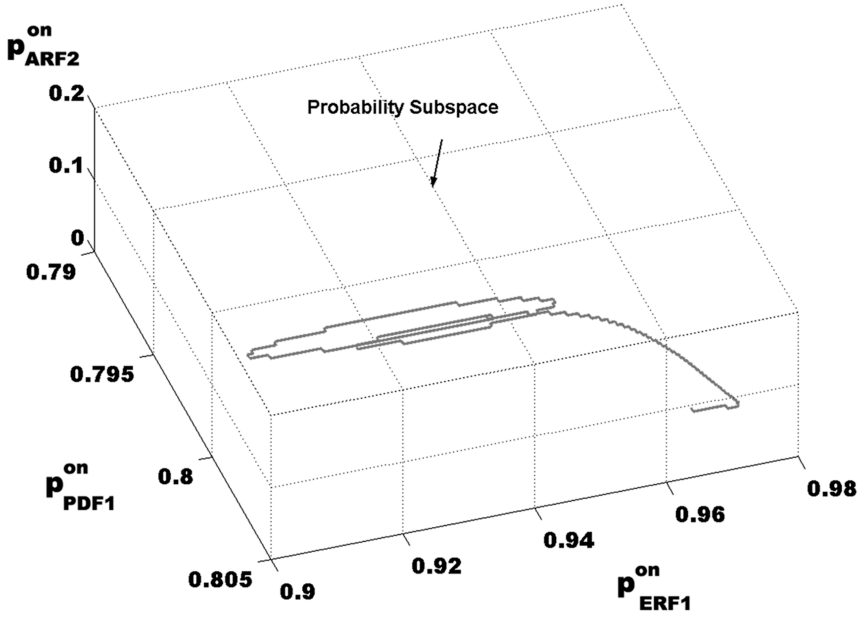

Fig. 7. Probability subspace generated by the fluctuations in in response to the slowly fluctuating input signal.

We also tested the dynamic features of the gene response to a chaotic temporal pattern of ethylene signaling. In this case, we simulated the effect of a signal that has a rapid chaotic temporal behavior on the probability of activating the three genes considered in the system. The signal was simulated by logistic chaos given by the equation $ET(i+1) = rET(i)(1-ET(i))$, with r = 3.99 and i = 0,1,2,3,..., and allowing changes in ethylene concentration every 0.04s (Fig. 8*A*). The response of the cell under such a situation is smooth rather than a reflection of the variations in the ethylene signal (Fig. 8*B*). Under a chaotic ethylene signaling behavior as the one simulated, the array of gene expression reaches the same attractor point (0.98, 0.80, 0) in the probability space (Fig. 8*C*) as that attained in absence of the chaotic signal for ET = 0.5μM (12μL/L). This

result suggests that under our assumptions, the activation of the genes considered responds to the average value of the signal and that the chaotic fluctuations around this value are either ignored or filtered out. The probability of activation of the three genes fluctuated and tended to a chaotic attractor only when the fluctuations were slow, suggesting that the system is unable to respond to input signals that fluctuate very rapidly (Figure 9 from *A* to *C*). This result is of theoretical relevance and it also makes novel predictions on how plants may respond to contrasting temporal patterns of signaling.

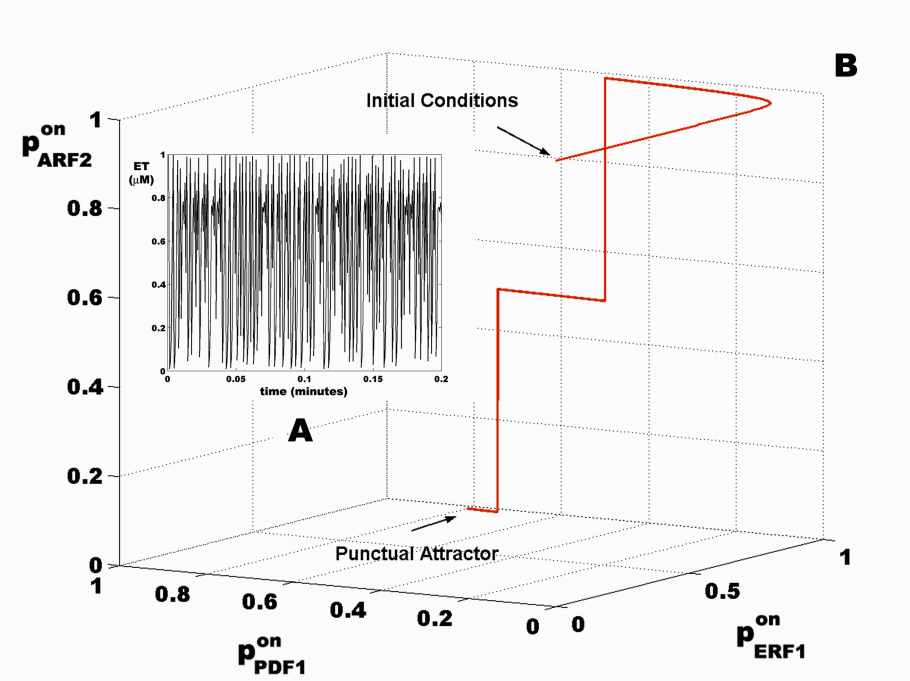

Fig. 8 (*A*) Chaotic logistic signal, represented by the function *ET(i+1) = rET(i)(1-ET(i))*, where *r* = 3.99 and *i* = 0, 1, 2, 3,…, with i changing every 0.04 s; (*B*) trajectory of the three-gene array in response to the chaotic signal. The trajectory is a smooth curve that drives the system to the attractor point (0.98, 0.80, 0), which is the same point under a steady concentration of 0.5 μM (12 μL/L) of ethylene.

Discussion

We present here a formal quantitative framework for simulating the activation response of a gene array involved in the *Arabidopsis* ethylene signaling and response pathway. The proposed approach can be applied to generate hypotheses on how a cell perceives and transduces ethylene signaling. Different ethylene concentrations and contrasting temporal regimes were tested for their effect on the activation responses of three important target genes. Our approach, or variations thereof, may be extended to other signaling and response pathways in both plant and animal cells.

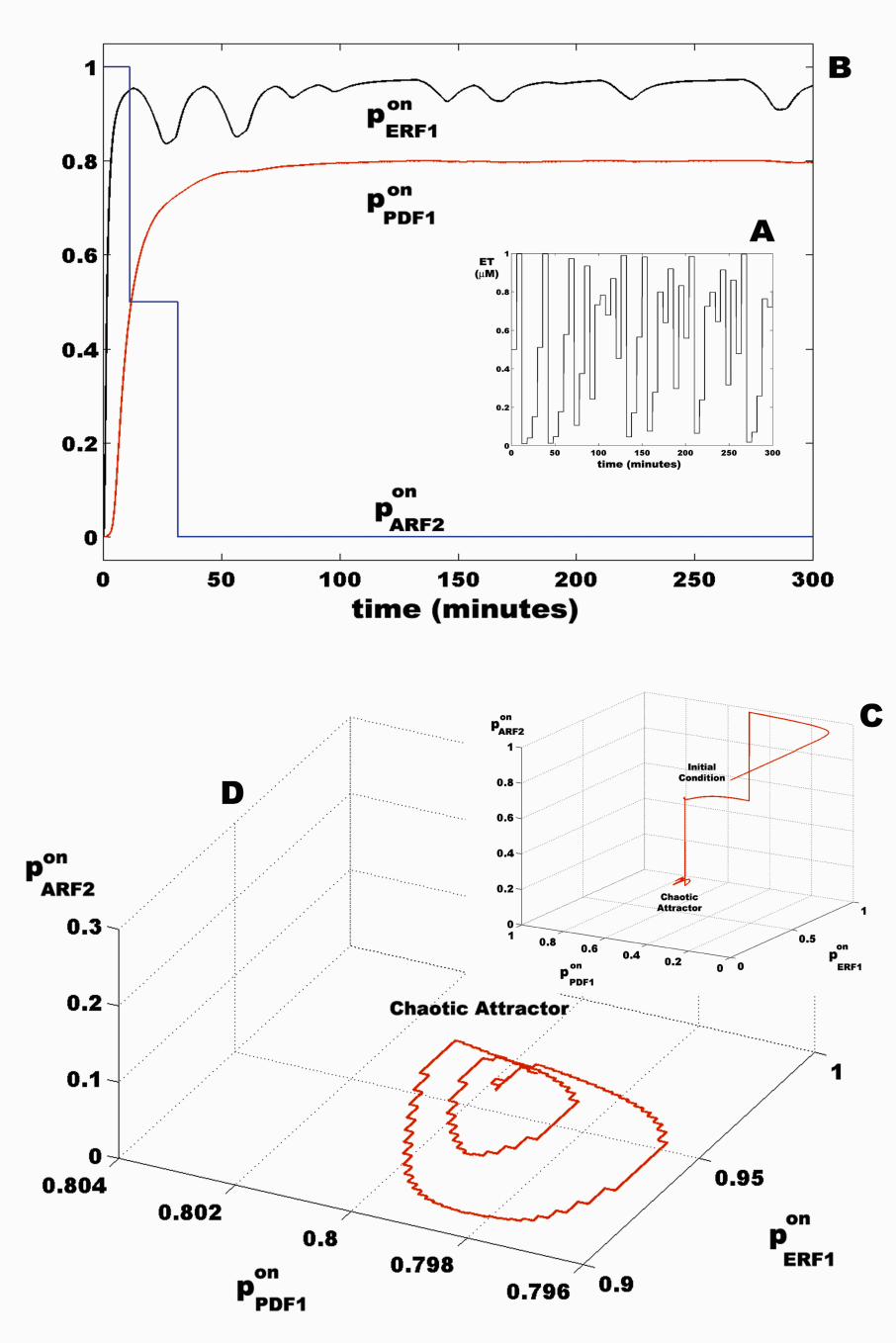

Fig. 9 (*A*) Chaotic logistic signal, represented by the function $ET(j+1) = rET(j)(1-ET(j))$, where $r = 3.99$, $j = 0, 1, 2, 3,\ldots$, with j changing each 360 s; (*B*) temporal response of the three-gene array to the chaotic signal, showing chaotic variations in p^{on}_{ERF1} in response to the input; (*C,D*) trajectory of the three-gene array in response to the chaotic signal. The trajectory is a smooth curve that drives the system to an attractor basin generated by the chaotic fluctuations in p^{on}_{ERF1}.

We have proposed 15 nonlinear differential equations that simulate temporal courses of the genetic response in *Arabidopsis* root cells to ethylene signaling. This set of equations

incorporates the dynamic features of the two modules that have been shown to constitute the ethylene signaling and response pathway in plant cells, and both the qualitative and the quantitative aspects of the model are grounded on available experimental data (see Table 1 and Appendix I: Model Section).

The model presented here for the MAPK cascade associated with the ethylene receptor suggests that this pathway in fact works as a molecular switch that is very stable even when part of the ETR is inactivated by the presence of ethylene (see Fig. 2). Based on this model, the threshold ethylene concentration needed to inactivate the cascade is in the order of 1μL/L; above this value, the cascade rapidly becomes inactive. Such a relatively high inactivation threshold value has important interesting physiological implications. According to the model, as ethylene concentration increases, the number of inactivated ETR molecules also increases and some of the EIN2 molecules of the nuclear membrane are activated (Guo & Ecke, 2004). Active EIN2 molecules allow the number of active EIN3 molecules in the nucleus to increase, which in turn activates the transcription of the ***ERF1*** gene, thereby generating the ethylene response.

As indicated in Fig. 3, the p_{ERF1}^{on} begins to increase at low ethylene concentrations above 0.001μL/L and reaches a plateau at ethylene concentrations above 10μL/L. Our analyses also suggest that *because the ethylene response is highly dependent on the activation of the **ERF1** gene, this range of probability values possibly underlies the form of the experimentally based curve observed in Chen and Bleecker* (1995). In addition, the results shown in Fig. *A1* of the Appendix I suggest an explanation for the intermediate phenotypes reported in the latter study of Chen and Bleecker (1995): these could correspond to states in which the MAPK cascade is not completely inactivated by ethylene and for which the ***ERF1*** gene is expressed at less than its full capacity. Therefore, *we predict that **ERF1** function is dose-dependent and that there should be a correlation between the phenotypes observed and the level of expression of this gene.*

The existence of CTR1 downstream components of the MAPK cascade in *Arabidopsis* ethylene pathway has been questioned (Stepanova & Alonso, 2005; Seger & Krebs, 1995; Ecker, 2004). Our results indicate that if the MAPKK and MAPK are actually in the ethylene reponse chain of reactions, these may function only as carriers that increase the fidelity and stability of the signal from CTR1 to EIN2. In this case, in the ethylene response, the set of phosphatases associated to their respective kinases that act along the chain of reactions could determine the rate and duration of the signal transmission, while the chain of phosphorylation reactions acting through the set of kinases could determine the amplitude of the transmitted signal (Huang & Ferrell, 1996; Kholodenko, 2000; Cho. & Wolkenhauer, 2003; Yamada, Taketomi & Yoshimura, 2004; Díaz & Martínez-Mekler, 2005). But all the conclusions derived from the model that does include the MAPKK and MAPK hold for the case that does not incorporate these.

The theoretical dose-response sigmoid curve obtained by our model is well adjusted by Eqn. [M.1], with a Hill coefficient of ~0.97 and a confidence range that includes the experimentally derived value of 0.99 in the phenotypic response curves obtained by Chen and Bleecker (1995) for mutants of upstream signaling components. Our model results thus suggest that such experimental curves could be due, at least in part, to ERF1 changes to different ethylene concentrations. Furthermore, this result suggests that the parameter values used in this paper are sufficiently close to the actual values in plant cells and that our model incorporates key

dynamical features of the actual ethylene signaling and response pathway. Although additional experimental work will be needed to obtain accurate estimates of the parameters of the dynamic system, our stability analysis (Appendix 2) strongly suggests that the overall qualitative postulates of our model should not be affected by variations in the estimates of the parameters. Therefore, we do not expect the actual parameter values to be orders of magnitude different from those proposed here.

Given that our ***ERF1*** dose-response curve was similar to that derived experimentally for the phenotype of the wild type plants; we proceeded to use our system to simulate the genetic responses of root cells subjected to different concentrations of ethylene and different temporal regimes of ethylene signaling by modeling the dynamics of the ERF1 protein that is synthesized under the action of ethylene. The model ignores the complex processing of the protein in the ER and allows us to estimate the accumulation rate of the ERF1 transcription factor in the nucleus. With the value of ERF1 in the nucleus, we were able to estimate N_{ERF1} and then used a Markov model to obtain p^{on}_{PDF1} for the activation of ***PDF1*** and p^{on}_{HLS1} for the activation of ***HLS1***. The activation of ***HLS1*** promotes the inactivation of ***ARF2*** (Section 6 of Table 1 and Appendix I). *This enabled us to link the temporal pattern of a stimulus - in this case eliciting an ethylene response - with the probability of expression of an array of genes that can mediate a particular cellular response to the original stimulus.*

Therefore, the model proposed here is a useful new tool that can simulate the dynamics of gene response to different concentrations and temporal regimes of signals. This approach can be applied to any characterized signaling and response pathway. We have particularly modeled the activation dynamics of ***ERF1*** in response to ethylene signaling, which in turn elicits the response of ***PDF1*** and the inhibition of ***ARF2***. In actual plant cells, ***ERF1*** is an activator or inhibitor of several other genes, and the response of the latter could also be modeled by extending the present model to a simulated genetic response that incorporates other genes in addition to the two considered here. In such a case, the array that records the states of activation of the genes would be of a higher dimension.

The promoter of ***PDF1*** contains a GCC box at which ERF1 binds, and the activation of ***PDF1*** induces the transcription of a defensin as part of the jasmonate-dependent defense response (Ton et al., 2002; Brown et al., 2003). The promoter of ***HLS1*** also has a GCC box at which ERF1 binds, and the activation of ***HLS1*** induces hook formation in darkness and functions as an integrator center for the ethylene, auxin and light pathways. ***HLS1*** negatively regulates the expression of the ***ARF2*** gene at a posttranslational level, avoiding the hook disruption due to ARF2 protein activity (Li et al., 2004).

The genes that we have chosen to model have been functionally characterized, and our approach provides several novel predictions and a dynamic and complementary interpretation of the phenotypes mediated by these genes under different ethylene signaling regimes. Figure 5 shows that the probability configuration adopted by the gene array is dependent on the concentration of ethylene applied to the system. In the absence of ethylene, the probability of ***ARF2*** expression is 1, and the probability of ***ERF1*** and ***PDF1*** expression is 0. This configuration corresponds to the point (0, 0, 1) in the probability space of the gene array (Fig. 5*A*) and to a phenotype in which root growth and hook formation is under the exclusive control of auxin and

in which the jasmonate-dependent defensive mechanism has not been activated. At 1.2μL/L of ethylene, the array moves to the point (0.35, 0.58, 0.5) in its probability space (Fig. 5*B*), which corresponds to a state of intermediate ***ERF1*** and ***PDF1*** expression and low ***ARF2*** expression. This state correlates with a phenotype in which root length and hook development are also controlled by ethylene and in which the jasmonate-dependent defensive mechanism is activated at an intermediate level. Finally, at 24μL/L of ethylene (Fig. 5*C*) the array moves to the point (0.98, 0.80, 0) in the probability space, which corresponds to a state of full expression of the ***ERF1*** and ***PDF1*** genes and complete inhibition of the ***ARF2*** gene expression. This state correlates with a triple response phenotype, including characteristics related to the ethylene response (Chang, 2003), while the role of auxin in root development and hook disruption is barely noticeable, and a full expression of the jasmonate-dependent defensive mechanisms is predicted.

The possibility of predicting the cell's dynamic genetic and phenotypic responses to variations in phytohormone concentrations will be the key to further understand the interconnections among signaling pathways and to predict the plant's responses to different hormone regimes. The theoretical approach proposed here has enabled in silico simulations of additional dynamic features of the cells genetic response to ethylene that are not commonly studied empirically and that provide novel predictions for future experimental tests.

We have shown (Figs. 6 and 7) that the gene array studied here has very interesting dynamical responses to different temporal regimes of ethylene signaling. Low- and high-frequency periodic variations in ethylene concentration produce small oscillations in the activation probability values of the genes studied. However, variations with a period value between 20min and 174min produce the transition between the maximum and minimum values of activation probability (p^{on}) for each gene. This is an unexpected prediction of our model that implies that only certain temporal regimes of environmental fluctuations can induce a high amplitude genetic response in the root cell. In addition, Fig. 6*B* clearly shows that under a periodic signal of ~35h the gene array shows a response that is confined to a cycle within its probability space. These results lead to the prediction that real root cells exposed to such a regime of ethylene signaling may transit through different observable gene expression profiles approximately every 35h, depending on other environmental conditions. Attempts at testing this and other related hypotheses that can be derived from the model's analyses experimentally should prove to be very interesting.

A more realistic situation corresponds to random fluctuations in ethylene concentrations. As a result, the trajectory drives the system into a confined probability subspace generated by p^{on}_{ERF1} (Fig. 7). In this case, only the gene immediately activated by the signaling cascade is affected by noise, while the probability of the *on* state of ***PDF*** and ***ARF2*** is not markedly affected by this non-Gaussian noise, suggesting that the complex translational machinery and protein processing of ERF1 in the ER filter out random fluctuations in the incoming signal. Thus, the phenotypes that are predicted to be expressed under random fluctuations in ethylene concentration are expected to be fairly similar to those observed under constant ethylene availability.

Chaos is a deterministic but irregular signal that can be used to obtain information on the full response capacity of the system because the trajectory of the system never goes through the same point in its phase space (Nicolis, 1995). In our case, the slow chaotic signal successfully induces the full capacity response of ***ERF1*** (Fig. 3), driving the system towards a chaotic attractor generated by this gene. However, the signal does not induce a chaotic response in ***PDF1*** and ***ARF2***, indicating that the response pathway that we have simulated, and which may very well reflect key aspects of the real cellular mechanisms, filters out any effect that this slow chaotic signal could have on the activation probability of the ***PDF1*** and ***ARF2*** genes. Thus, the phenotypes elicited under the command of these two genes would not be significantly affected under such a temporal signaling regime. A similar result is obtained for different values of the parameter r in the chaotic window of the logistic equation $ET(i+1) = rET(i)(1-ET(i))$ with i = 0,1,2,3,…(data not shown). Further simulations would still be required to fully characterize the dynamic response of the system to chaotic signals, but this is out of the scope of the present work.

Acknowledgements
We thank Dr. P. Padilla, C. Espinosa, M. Benítez, A. Chaos and E.Ortiz for useful discussions and suggestions to this work during the Theoretical Biology Group seminars of our Laboratory in Mexico. E.A.B. also acknowledges an International Fellowship from the Santa Fe Institute (SFI) where parts of this work were completed. D. Krakauer and N. Fedoroff affiliated to the SFI inspired aspects of this work and helped improve it, respectively. Financial support was from PAPIIT (Programa de Apoyo a Proyectos de Investigación e Innovación Tecnológica), UNAM (Universidad Nacional Autónoma de México; IN 230002 and IN212995) and CONACYT (Consejo Nacional de Ciencia y Tecnología; 41848-Q and 31871-N) grants to E.A.B

APPENDIX 1: Model

Root cell modeled as a three-compartmental system

The ethylene receptor, which appears to be located in the endoplasmic reticulum (ER) membrane of the root cell, induces a chemical reaction that is located inside the lumen of the ER, with a volume V_{ER}. This volume, considered in the model to be the first compartment, can be used to model the concentration of all the signaling molecules of the MAPK cascade. The inactivation of the ethylene receptors induces the activation of a series of transcriptional processes in the nucleus of the root cell, which can be considered to be the second compartment, with a volume of $V_{nucleus}$. Both compartments are enclosed in a rectangular cylindrical cell with a diameter of 30 μm and a height of 10 μm; this space can be taken to be the third compartment.

In plants, the ER shows very complex spatio-temporal dynamical features that are not observed in animal cells (Matsushima et al., 2002; Galili, 2004; Hara-Nishimura et al., 2004). The presence of compartments attached to the main structure of the ER produces a membranous structure whose geometry is difficult to model (Hara-Nishimura, et al., 2004). However, we assume that the set of reactions of the MAPK module occurs inside the ER main body and that this main body can be modeled as a cylinder with a diameter of 1 μm and a height of 10 μm (Galili, 2004). Consequently, V_{ER} has a value of 7.86 μm^3 (7.86 x 10^{-15} l) in our model.

The nucleus can be modeled as a sphere with a diameter of 10 μm, which implies that $V_{nucleus}$ has a value of 524 μm^3 (5.24 x 10^{-13} l). The concentrations of the molecules that are transported from the ER to the nucleus, and vice versa, can now be described by the ratio $V_{nucleus}/V_{ER}$, which based on our values is 66.5. Assuming that the concentration of molecule k in the ER at time t is $c_k(t)$, then if this molecule is moved into the nucleus (either by diffusion or by transport of any kind) its concentration would be:

$$C_k(t) = c_k(t)V_{ER} / V_{nucleus} \qquad [1]$$

Thus, the concentration of molecule k in the ER is 0.015-fold lower than in the nucleus. Likewise, for movements in the opposite direction, the concentration of a molecule k will be 66.6-fold higher with respect to its concentration in the ER (see Table 1, Section 5).

Activation of the MAPK module

In the model, we assume that the total concentration of ethylene receptors in the ER membrane (denoted by ETR_T) is ~ 0.3 μM (which is equivalent to ~1,400 molecules of the receptor). The activated state of the receptor is denoted by $ETR^{(+)}$ and its inactivated state by $ETR^{(-)}$. In the absence of ethylene, all receptors are in their constitutive activated state, and $ETR^{(+)} = ETR_T$. In the presence of ethylene, both states obey the balance equation:

$$ETR^{(+)} + ETR^{(-)} = ETR_T \qquad [2]$$

In this form, if we use *CTR1** to denote the concentration of the activated constitutive triple response 1 molecule and *MAPKK** and *MAPK** to denote the activated state of the kinases downstream of CTR1*, we obtain the following balance equations for the activation rates of the kinases that conform to the MAPK module at the ER lumen of the root cell:

$$\frac{dCTR1^*}{dt} = \kappa_3 \left(ETR_T - ETR^{(-)} \right) \left(CTR1_T - CTR1^* \right) - \kappa_4 CTR1^* \qquad [3]$$

$$\frac{dMAPKK^*}{dt} = \kappa_5 CTR1^* \left(MAPKK_T - MAPKK^* \right) - \kappa_6 MAPKK^* \qquad [4]$$

$$\frac{dMAPK^*}{dt} = \kappa_7 MAPKK^* \left(MAPK_T - MAPK^* \right) - \kappa_8 MAPK^* \qquad [5]$$

Equation [3] indicates that the velocity of activation of CTR1 is directly proportional to the product of the concentration of activated ETR and to the amount of inactivated CTR1 molecules minus the rate of deactivation of the activated CTR1 molecule. We assume that one activated CTR1 molecule is associated at each and every moment to the activated ETR; thus, $CTR1_T \sim 0.3$ μM in our model. The value of the κ_3 rate constant of Eqn. [3] was adjusted by assuming that at zero ethylene concentration all of the CTR1* molecules are in a steady activated state. The value of κ_4 was based on the observations of Chen and Bleecker (1995) that at very low values of ethylene concentration (<<0.001 μL/L) almost all of the CTR1 molecules are in their steady activated state. The values of these parameters for $CTR1^* \sim 0.29$ μM for low ethylene concentrations are given in Table 1, Section 7.

The activation of the kinases downstream of CTR1* (Fig. 1 of main article) are modeled following Yamada, Taketomi and Yoshimura (2004) and Diaz and Martinez-Mekler (1995), giving rise to Eqns. [4] and [5]. In these equations, $MAPKK_T$ and $MAPK_T$ are assumed to be ~0.5 μM (7), which is equivalent to a total amount of ~2,370 molecules of each kinase in the ER. Equation [4] indicates that the rate of activation of the MAPKK is a balance between its rate of activation by CTR1* and its rate of inactivation by its phosphatase. Equation [5] indicates that the rate of activation of the MAPK is a balance between its rate of activation by MAPKK* and its rate of inactivation by its phosphatase.

The values of the rate constants of Eqns. [4] and [5] are taken from Yamada et al. (2004), assuming, as a first approximation, that the kinetics of activation of the MAPKK and MAPK molecules in the *Arabidopsis* cells is very similar to that observed for MEK and ERK in animal cells (see Table 1).

Inactivation of EIN2

MAPK* blocks the EIN2 molecule of the nuclear membrane (main article: Fig. 1) at a rate given by:

$$\frac{dEIN2^{(-)}}{dt} = \kappa_9 MAPKc^* \left(EIN2_T - EIN2^{(-)} \right) - \kappa_{10} EIN2^{(-)} \frac{ETR^{(-)}}{ETR^{(-)} + \beta} \qquad [6]$$

where $EIN2^{(-)}$ represents the concentration of inactivated EIN2 in the nucleus and $EIN2_T$ its total concentration. According to the above equation, the rate of inactivation of EIN2 is a balance between its rate of phosphorylation by MAPK* and its rate of dephosphorylation by a still

unknown process. However, we assume that it depends on the rate of inactivation of the ethylene receptors according to a Michaelis-Menten behavior.

In this equation, we assume that the total concentration of EIN2 (denoted by $EIN2_T$) is 0.005 μM with respect to the nucleus, which is equivalent to ~1,580 molecules of the channel. In the absence of ethylene, all of the EIN2 molecules are in their phosphorylated state; thus, $EIN2^{(-)} = EIN2_T$. We then adjust the rate constants in order to obtain $EIN2^{(-)} \approx EIN2_T \approx 0.005$ μM for very low concentrations of ethylene (<<0.001 μL/L) because the response of the system to ethylene is minimal at these concentrations (Chen & Bleecker, 1995). For other ethylene concentrations, the number of inactivated EIN2 molecules slowly decreases according to the balance equation, $EIN2^{(-)} + EIN2^{(+)} = EIN2_T$. Consequently, at high concentrations of ethylene (>10 μL/L), all of the EIN2 molecules are in their dephosphorylated state and $EIN2^{(+)} = EIN2_T$. The respective values of the rate constants of Eqn. [6] are shown in Table 1, Section 7.

*MAPKc** represents the corrected concentration of the activated MAPK with respect to the nuclear volume in Eqn. [6]. The form in which this concentration is scaled is shown in the Table 1, Section 5.

Inactivation of the MAPK cascade and activation of the ethylene response

Inactivation of the MAPK cascade occurs when the ethylene gas binds to either of its specific receptors at a rate proportional to the amount of ethylene gas still unbound and to the number of receptor molecules that are still in their activated state (Figure A1). Thus, the rate of inactivation of the receptor is given by:

$$\frac{dETR^{(-)}}{dt} = \kappa_1 (ET - ETR^{(-)})\left(ETR_T - ETR^{(-)}\right) - \kappa_2 ETR^{(-)} \qquad [7]$$

where ET represents the total amount of ethylene gas, which is a control parameter. This equation is subject to balance equation [2]. The values of the rate constants of Eqn. [7] were obtained from the work of Chen and Bleecker (1995) in that at very high concentrations of ethylene (>10 μL/L), the MAPK cascade should be completely inactivated; thus, $ETR^{(-)} \sim 0.3$ μM. These values are shown in the Table 1.

Once the MAPK has been blocked by the presence of ethylene, the EIN2 molecule of the nuclear membrane (main article, Fig. 1) is activated at a rate given by:

$$\frac{dEIN2^{(+)}}{dt} = -\frac{dEIN2^{(-)}}{dt} \qquad [8]$$

subject to $EIN2^{(-)} + EIN2^{(+)} = EIN2_T$ (see Eq. [6] above).

Once EIN2 has been activated (dephosphorylated), the EIN3 molecule inside the nucleus is activated by a still unknown process (8) at a rate given by:

$$\frac{dEIN3*}{dt} = \kappa_{11} EIN2^{(+)} \left(EIN3_T - EIN3* \right) - \kappa_{12} E1N3* \quad [9]$$

where $EIN3*$ is the concentration of the activated form of the EIN3 transcription factor in the nucleus, and $EIN3_T$ is the total concentration of the molecule in the nucleus. We assume that $EIN3_T$ = 0.005 μM, which is equivalent to ~1,580 molecules, which has been taken to be the size of the pool of this molecule in the nucleus. The rate constants in Eqn. [9] were adjusted in order to obtain a value of EIN3* ~ 0.005 μM for high concentrations of ethylene. (See Table 1, Section 7).

The activated EIN3 transcription factor binds to the promoter site of the *ERF1* gene, thereby allowing its expression. The two-state Markov model for this process is given by the equations:

$$\frac{dp^{on}_{ERF1}(t)}{dt} = \kappa_{13} N_{EIN3*} p^{off}_{ERF1}(t) - \kappa_{14} p^{on}_{ERF1}(t)$$

$$\frac{dp^{on}_{ERF1}(t)}{dt} = -\kappa_{13} N_{EIN3^*} p^{off}_{ERF1}(t) + \kappa_{14} p^{on}_{ERF1}(t) \quad [10]$$

where the rate constants were chosen from a set of values for which $p^{on}_{ERF1} > 0.95$ when the concentration of ethylene is greater than 10 μL/L (see Table 1, Section 7). In the absence of ethylene, the *ERF1* gene is in the *off* state with a probability 1. The number of activated EIN3* molecules for these equations can be easily calculated as:

$$N_{EIN3*} = \left(1x10^{-21} \right) EIN3* V_{nucleus} N_{Avogadro} \quad [11]$$

Activation of target genes downstream *ERF1*

Once the *ERF1* gene has been activated in response to ethylene, it is transcribed, as a first approximation, at a rate given by:

$$\frac{dmRNA}{dt} = \frac{p^{on}_{ERF1}(t) V_{trans} mRNA}{mRNA + \kappa_{15}} - \kappa_{16} mRNA \quad [12]$$

where $mRNA$ is the nuclear concentration of the transcripts of the *ERF1* gene, and V_{trans} is the maximum transcription rate of *EFR1* (see Table 1, Section 7), which is obtained when p^{on}_{ERF1} = 1. According to Goutsias and Kim (2004), the transcription rate for mRNA is of the order of 0.0001 pM s^{-1} to 1 pM s^{-1}. We used a slightly higher value of 0.000003 μM s^{-1} (3 pM s^{-1}) in order to obtain a steady pool of a rounded-off number of mRNA molecules in the nucleus (~1,000); this value is also obtained when the values reported in the Table 1, Section 7, for the other rate constants of Eqn. [12] are taken into consideration.

The rate of production of the ERF1 protein is then:

$$\left.\frac{dERF1}{dt}\right|_{ER} = \kappa_{17} mRNA - D_{erf1} ERF1 \qquad [13]$$

where k_{17} is the translation rate and $D_{erf1}ERF1$ is the amount of ERF1 protein moved (by some yet unknown mechanism) from the ER into the nucleus. According to Goutsias and Kim (2004), k_{17} has an estimated value between 0.05 s^{-1} and 0.20 s^{-1}. In our model, we considered a value of 0.1972 s^{-1} (see Table 1, Section 7), for which the number of ERF1 molecules in ER is also ~1,000 molecules at an ethylene concentration of greater than 10 μL/L.

In the nucleus and following an adjustment of the corresponding concentration (see Table 1, Section 5), the amount of ERF1 varies according to the balance equation:

$$\left.\frac{dERF1}{dt}\right|_{nucleus} = D_{erf1} ERF1n - \kappa_{18} ERF1n \qquad [14]$$

where the first term of the right side of Eqn. [14] represents the amount of ERF1 moved from the ER into the nucleus (*ERF1n*), and the second term represents the degradation of the protein. In the model, we assigned the value of 0.99 s^{-1} to D_{erf1}; at this value, most of the ERF1 molecules produced in the ER are moved into the nucleus. k_{18} is then adjusted to obtain a steady concentration of ~1,000 ERF1 molecules for high concentrations of ethylene (see Table 1, Section 7).

Finally, we can then model, as a first approximation, the activation of the ***PDF1*** gene with a two-state Markov model given by:

$$\begin{aligned} \frac{dp^{on}_{PDF1}(t)}{dt} &= \kappa_{19} N_{ERF1n} p^{off}_{PDF1}(t) - \kappa_{20} p^{on}_{PDF1}(t) \\ \frac{dp^{off}_{PDF1}(t)}{dt} &= -\kappa_{19} N_{ERF1n} p^{off}_{PDF1}(t) + \kappa_{20} p^{on}_{PDF1}(t) \end{aligned} \qquad [15]$$

The inactivation of the ***HLS1*** gene is given by another two-state Markov model:

$$\begin{aligned} \frac{dp^{on}_{HLS1}(t)}{dt} &= \kappa_{21} N_{ERF1n} p^{off}_{HLS1}(t) - \kappa_{22} p^{on}_{HLS1}(t) \\ \frac{dp^{off}_{HLS1}(t)}{dt} &= -\kappa_{21} N_{ERF1n} p^{off}_{HLS1}(t) + \kappa_{22} p^{on}_{HLS1}(t) \end{aligned} \qquad [16]$$

where N_{ERF1n} is calculated as indicated in the Table 1, Section 4 in the main article.

With respect to Eqns. [15] and [16], the value of the rate constants were adjusted to obtain a $p^{on} > 0.75$ for high ethylene concentrations (>10 μL/L) (see Table 1, Section 7).

As we do not know the posttranslational mechanism by which the expression of the gene ***ARF2*** is negatively regulated by the ***HLS1*** gene (Li et al., 2004) we modeled the expression of ***ARF2*** as a three-state discrete variable given by:

$$p^{on}_{ARF2}(t) = \begin{cases} 0 & \text{if } p^{on}_{HLS1}(t) > 0.75 \\ 0.5 & \text{if } 0.5 < p^{on}_{HLS1}(t) \le 0.75 \\ 1 & \text{if } p^{on}_{HLS1}(t) \le 0.5 \end{cases} \qquad [17]$$

Thus, according to Eqn. [17], if ***HLS1*** is fully expressed at time *t*, the probability of expression of ***ARF2*** is 0 at time *t*. In this form, we are combining a continuous approach (***HLS1*** activation) with a three-state, time-dependent discrete approach (***ARF2*** negative regulation).

If we remove Eqns. [4] and [5] from the set of equations, the dynamical features of the model do not change. See Figs. 2*B* and 3*B* in the Main Article and compare them with Figs 2A and 3A in the Main Article, indicating that the role of the kinases downstream of CTR1, if they exist, is only to transmit the signal from the ETR to EIN2.

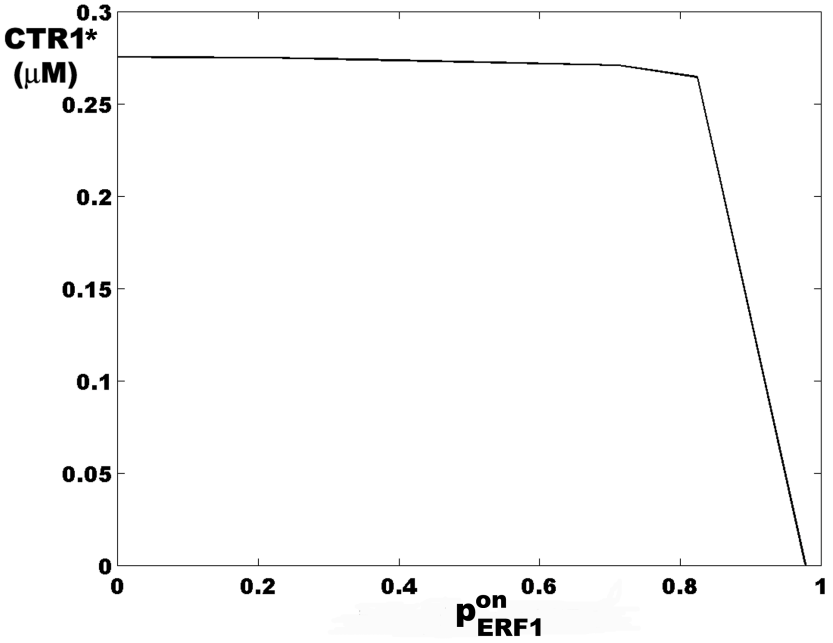

Figure A1.- Phase portrait for the dependence of p_{ERF1}^{on} on $CTR1^{*}$. This plot shows that the full expression of the ethylene response is obtained only when the MAPK cascade in the ER has been completely inactivated. The model predicts the coexistence of the effects of the MAPK cascade with those of the ethylene response that can give rise to a series of intermediate phenotypes that could be observed experimentally.

Appendix 2:

In this section we perform the stability analysis of the model for the ethylene response. The 8 equations for *ETR*, *CTR1*, *MAPKK*, *MAPK*, *EIN2*, *EIN3*, p_{ERF1}^{off} and p_{ERF1}^{on} (see Sections from 1 to 4 of Table 1 in the main article) are the model's core and the stability of these equations determines the global stability of the model.

According to Table 1 in the main text the steady state values for these variables are:

$$ETR^{(-)^0} = \frac{\gamma}{2} - \frac{\sqrt{\gamma^2 - 4\left(ET\right)\left(ETR_T\right)}}{2} \qquad [A1]$$

$$\gamma = ET + ETR_T + \frac{\kappa_2}{\kappa_1}$$

$$CTR1^{*0} = \frac{\left(ETR_T - ETR^{(-)^0}\right)CTR1_T}{\left(ETR_T - ETR^{(-)^0}\right) + \frac{\kappa_4}{\kappa_3}} \qquad [A2]$$

$$MAPKK^{*0} = \frac{CTR1^{*0}\ MAPKK_T}{CTR1^{*0} + \frac{\kappa_6}{\kappa_5}} \qquad [A3]$$

$$MAPK^{*0} = \frac{MAPKK^{*0}\ MAPK_T}{MAPKK^{*0} + \frac{\kappa_8}{\kappa_7}} \qquad [A4]$$

$$EIN2^{(-)^0} = \frac{MAPKc^{*0}\ EIN2_T}{MAPKc^{*0} + \frac{\kappa_{10}}{\kappa_9}\frac{ETR^{(-)^0}}{ETR^{(-)^0} + \beta}} \qquad [A5]$$

where

$$EIN3^{*0} = \frac{EIN2^{(+)^0}\ EIN3_T}{EIN2^{(+)^0} + \frac{\kappa_{12}}{\kappa_{11}}} \qquad [A6]$$

$$p_{ERF1}^{on^0} = \frac{N_{EIN3}^0}{N_{EIN3}^0 - \frac{\kappa_{14}}{\kappa_{13}}} \qquad [A7]$$

where $N_{EIN3}^0 = 602.3 V_{nucleus} EIN3^{*0}$

$$p_{ERF1}^{off^0} = 1 - p_{ERF1}^{on^0} \qquad [A8]$$

and the set of linearized equations around the steady state point of the system is, according to Table 1 in the main article:

$$\frac{d\delta\mathbf{e}}{dt} = \mathbf{J}\delta\mathbf{e} \qquad [A9]$$

where

$$\delta\mathbf{e} = \begin{bmatrix} \delta ETR^{(-)} \\ \delta CTR1^* \\ \delta MAPKK^* \\ \delta MAPK^* \\ \delta EIN2^{(-)} \\ \delta EIN3^* \\ \delta p_{ERF1}^{on} \\ \delta p_{ERF1}^{off} \end{bmatrix} \qquad [A10]$$

subject to:

$$\delta ETR^{(-)} = -\delta ETR^{(+)}$$

$$\delta EIN2^{(-)} = -\delta EIN2^{(+)}$$

$$\delta MAPKc^* = 0.00954\delta MAPK^*$$

and **J** is the Jacobian matrix of the linearized system given by:

$$\mathbf{J} = \begin{bmatrix} J_{11} & 0 & 0 & 0 & 0 & 0 & 0 & 0 \\ J_{21} & J_{22} & 0 & 0 & 0 & 0 & 0 & 0 \\ 0 & J_{32} & J_{33} & 0 & 0 & 0 & 0 & 0 \\ 0 & 0 & J_{43} & J_{44} & 0 & 0 & 0 & 0 \\ J_{51} & 0 & 0 & J_{54} & J_{55} & 0 & 0 & 0 \\ 0 & 0 & 0 & 0 & J_{65} & J_{66} & 0 & 0 \\ 0 & 0 & 0 & 0 & 0 & 0 & J_{77} & J_{78} \\ 0 & 0 & 0 & 0 & 0 & 0 & J_{87} & J_{88} \end{bmatrix} \qquad [A11]$$

where:

$$J_{11} = -\left[\kappa_1\left(ET + ETR_T - 2ETR^{(-)^0}\right) - \kappa_2\right]$$

$$J_{21} = -\kappa_3\left(CTR_T - CTR1^{*^0}\right)$$

$$J_{22} = -\left(\kappa_3 ETR^{(+)^0} + \kappa_4\right)$$

$$J_{32} = \kappa_5\left(MAPKK_T - MAPKK^{*^0}\right)$$

$$J_{33} = -\left(\kappa_5 CTR1^{*^0} + \kappa_6\right)$$

$$J_{43} = \kappa_7\left(MAPK_T - MAPK^{*^0}\right)$$

$$J_{44} = -\left(\kappa_7 MAPK^{*^0} + \kappa_8\right)$$

$$J_{51} = -\kappa_{10} EIN2^{(-)^0}\frac{\beta}{\left(ETR^{(-)^0} + \beta\right)^2}$$

$$J_{54} = 0.00954\kappa_9\left(EIN2_T - EIN2^{(-)^0}\right)$$

$$J_{55} = -\left[0.00954\kappa_9 MAPK^{*^0} + \frac{\kappa_{10} ETR^{(-)^0}}{ETR^{(-)^0} + \beta}\right]$$

$$J_{65} = -\kappa_{11}\left(EIN3_T - EIN3^{*^0}\right)$$

$$J_{66} = -\left(\kappa_{11} EIN2^{(+)^0} + \kappa_{12}\right)$$

$$J_{77} = -\kappa_{13} N^0_{EIN3}$$

$$J_{78} = \kappa_{14}$$

$$J_{87} = \kappa_{13} N^0_{EIN3}$$

$$J_{88} = -\kappa_{14}$$

The characteristic equation of the Jacobian matrix [A11] is given by:

$$\left|\mathbf{J} - \lambda\mathbf{I}\right| = 0 \qquad \text{[A12]}$$

which leads to:

$$\left(J_{11} - \lambda\right)\left(J_{22} - \lambda\right)\left(J_{33} - \lambda\right)\left(J_{44} - \lambda\right)\left(J_{55} - \lambda\right)\left(J_{66} - \lambda\right)\left[\left(J_{77} - \lambda\right)\left(J_{88} - \lambda\right) - J_{78}J_{87}\right] = 0 \qquad \text{[A13]}$$

Equation [A13] was numerically solved for each ethylene concentration from 0 to 10μM (0 to 240μL/L) and in Figure A2 we show the behavior of the eight eigenvalues obtained from the characteristic equation solution.

Figure A2 shows that all the eigenvalues of the linearized system remains upper bounded

by zero, i.e., $\lambda_j \leq 0$, j = 1, 2, 3,...,8, for each ethylene concentration, which indicates that the steady state reached by the system is stable against small perturbations in every case. Thus, under each ethylene concentration the system evolves towards a stable point attractor in the 8-dimension phase space.

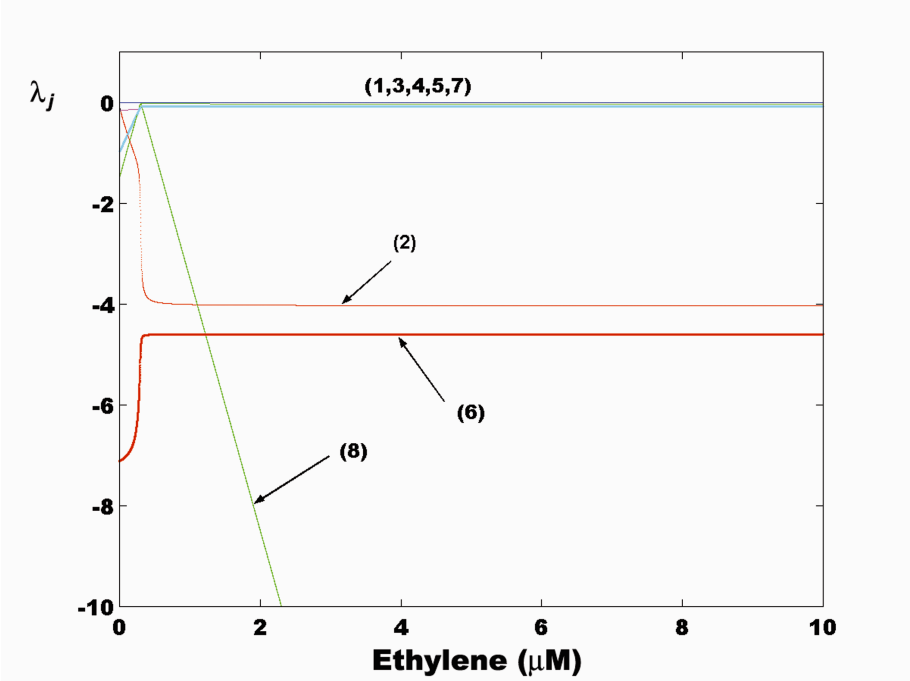

Figure A2.- Eigenvalues as a function of Ethylene concentration from the characteristic equation of the linearized system of equations of the ethylene model. The number in the parenthesis represents the corresponding eigenvalue at each ethylene concentration.

A possible weak aspect of our model is that we do not have accurate estimates of the parameters and that these are prone to stochastic variation in biological systems. Hence it is important to test the model's behavior under different value estimates. We addressed this by numerically solving equation [A13] assuming that all parameter values considered were random variables. However, we focus this analysis in three equations that are fundamental for the global dynamics of the system: activation of the ETR and of the CTR1 molecule in the ER and activation of EIN2 in the nucleus.

These three processes are the key ones for the expression of the phenotypic characteristics of the root cell and command the state of activation of the MAPK in the ER lumen and of the genetic ERF1-dependent machinery in the nucleus. Thus, it is very important to know if the steady states predicted for the genes activation differential equations in the model hold for all the parameter phase state space, or depend on the parameter values used and a few others. The latter situation would greatly limit the descriptive and predictive power of our model.

We analyzed effects of random fluctuations in κ_1 and κ_2 that command the activation of the ETR; in κ_3 and κ_4 that command the activation of the CTR1 molecule and in κ_9 and κ_{10} that command the activation of the EIN2 molecule. The ranges tested were from 0 to 15μM^{-1} s^{-1} for κ_1, κ_3 and κ_9; from 0 to 0.01s^{-1} for κ_2, and from 0 to 0.015s^{-1} for κ_4 and κ_{10}. In the latter we allowed the random variation of β that commands the activation of the EIN2 molecule allowing a

variation between 0 and 15μM. The ranges considered included the parameter values that we used in the model (see Table 1 Supporting). Ethylene concentration was varied from 0.12μL/L to 120μL/L and for each ethylene concentration 6000 parameter values for each couple of parameters was tested.

In all cases the global behavior of the eigenvalues remained bounded by zero and was not affected as we show in the example presented in figure A3.

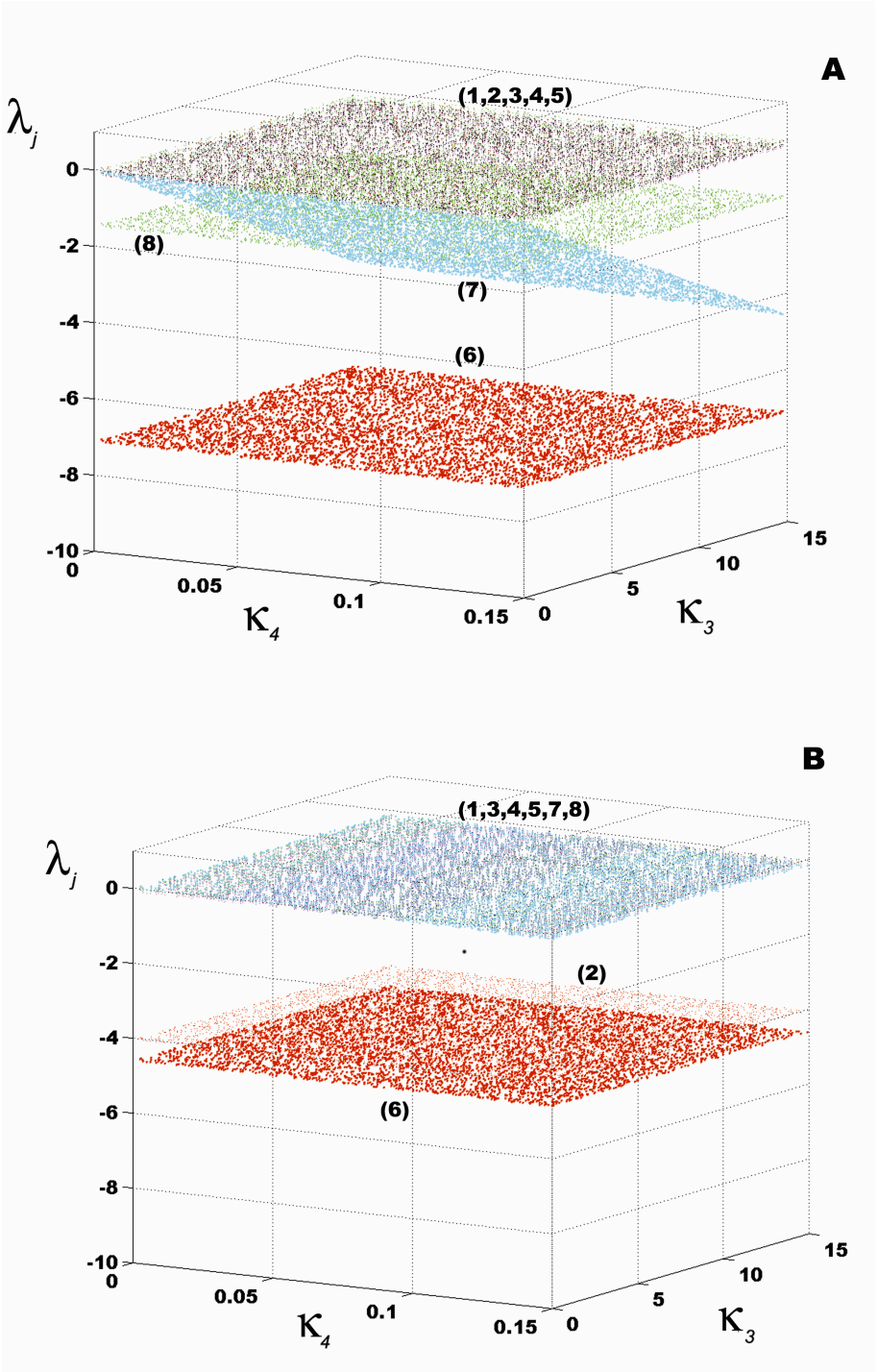

Figure A3.- Example of the results obtained from the random variation in each couple of parameter values of the equations indicated in the text. (a) Eigenvalues of the linerized system under stimulation with 0.005µM (0.12µL/L) of ethylene; (b) Eigenvalues of the linerized system under stimulation with 5µM (120µL/L) of ethylene. In both panels κ_3 was randomly varied from 0 to 15$\mu M^{-1}s^{-1}$ and κ_4 from 0 to 0.15s^{-1}. The number in parenthesis indicates the respective eigenvalue. In this figure we show only two values of the range of ethylene concentration used during the analysis (0.12µL/L to 120µL/L).

The above analysis clearly shows that the model we present in this work is stable against perturbations in the key parameters values, i.e., there are no instabilities for a wide range of parameter values of the system, or bifurcation points that could lead the system to an unexpected qualitative behavior not considered during the formulation of the model.

The particular set of parameter values that we chose for our model is included in the above analyses and this makes us more confident that the model thoughtfully reflects the real molecular dynamics of the ethylene response in the *Arabidopsis* root cell, in spite of the uncertainty on the estimates of the parameters. These results suggest that more precise estimates of the parameter will not affect our results in a significant way.

References

Albert, R. & Othmer, G. (2003). The topology of the regulatory interactions predicts the expression pattern of the segment polarity genes in Drosophila melanogaster. *J. Theor; Biol.* 223, 1-18.

Bleecker, A., Esch, J., Hall, A., Rodriguez, F. & Binder, B. (1998) The ethylene-receptor family from *Arabidopsis*: structure and function. *Philos. Trans. R. Soc. London Ser. B* 353, 1405-1412.

Brown, R., Kazan, K., McGrath, K., Maclean, D. & Manners, J. (2003) A Role for the GCC-Box in Jasmonate-Mediated Activation of the *PDF1.2* Gene of Arabidopsis. *Plant Physiol.* 132**,** 1020–1032.

Chang, C. & Stadler, R. (2001) Ethylene hormone receptor action in Arabidopsis. *BioEssays* 23, 619-627.

Chang, C. (2003) Ethylene signaling: the MAPK module has finally landed. *TRENDS in Plant Science* 8, 365-368.

Chen, Q. & Bleecker, A. (1995) Analysis of Ethylene Signal-Transduction Kinetics Associated with Seedling-Growth Response and Chitinase Induction in Wild-Type and Mutant Arabidopsis. *Plant Physiol.* 108**,** 597-607.

Cho, K. & Wolkenhauer, O. (2003) Analysis and modelling of signal transduction pathways in systems biology. *Biochem. Soc. Trans.* 31, 1503-1509.

Díaz, J. & Martínez-Mekler, G. (2005) Interaction of the IP3–Ca2+ and MAPK signaling systems in the *Xenopus* blastomere: a possible frequency encoding mechanism for the control of the *Xbra* gene expression. *Bull. Math. Biol.* 67, 433-465.

Ecker, J. R. (2004) Reentry of the Ethylene MPK6 Module. *Plant Cell* 16**,** 3169–3173.

Espinosa-Soto, C., Padilla-Longoria, P. & Alvarez-Buylla, E. (2004) A gene regulatory network model for cell-fate determination during *Arabidopsis thaliana* flower development that is robust and recovers experimental gene expression profiles. *Plant Cell* 16, 2923-2939.

Galili, G. (2004) ER-Derived Compartments Are Formed by Highly Regulated Processes and Have Special Functions in Plants. *Plant Physiol.* 136, 3411–3413.

Goutsias, J. & Kim, S. (2004) A Nonlinear Discrete Dynamical Model for Transcriptional Regulation: Construction and Properties. *Biophys. J.* 86, 1922-1945.

Guo, H. & Ecke, J. (2004) The ethylene signaling pathway: new insights. *Current Opinion in Plant Biology* 7, 40–49.

Hara-Nishimura, I., Matsushima, R., Shimada, T. & Nishimura, M. (2004) Diversity and Formation of Endoplasmic Reticulum-Derived Compartments in Plants. Are These Compartments Specific to Plant Cells? *Plant Physiol.* 136, 3435–3439.

Huang, C. & Ferrell, J. (1996) Ultrasensitivity in the mitogen-activated protein kinase cascade. *Proc. Natl. Acad. Sci. USA*. 93, 10078–10083.

Kholodenko, B. (2000) Negative feedback and ultrasensitivity can bring about oscillations in the mitogen activated protein kinase cascades. *Eur. J. Biochem.* **267,** 1583–1588.

Kieber, J. (1997) The ethylene response pathway in Arabidopsis. *Annu. Rev. Plant Physiol. Plant Mol. Biol.* 48**,** 277–96.

Li, H., Johnson, P., Stepanova, A., Alonso, J. M. & Ecker, J. R. (2004) Convergence of Signaling Pathways in the Control of Differential Cell Growth in Arabidopsis. *Dev. Cell* 7**,** 193–204.

Lorenzo, O., Piqueras, R., Sánchez-Serrano, J. J. & Solano, R. (2003) *ETHYLENE RESPONSE FACTOR1* integrates signals from ethylene and jasmonate pathways in plant defense. *Plant Cell* 15, 165–178.

Matsushima R, Hayashi Y, Kondo M, Shimada T, Nishimura M, and Hara-Nishimura I (2002) An Endoplasmic Reticulum-Derived Structure That Is Induced under Stress Conditions in Arabidopsis**.** *Plant Physiol.* 130, 1807–1814.

Mendoza, L. & Alvarez-Buylla, E. R. (2000) Genetic Regulation of Root Hair Development in *Arabidopsis Thaliana*: A Network Model. *J. Theor. Biol.* 204, 311-326

Nicolis, G. (1995) *Introduction to nonlinear science.* Cambridge University Press, Cambridge.
Perkins, J., Hallett, M. & Glass, L. (2004). Inferring models of gene expression dynamics. *J. Theor. Biol.* 230**,** 289–299.

Seger, R. & Krebs, E. (1995) The MAPK signaling cascade. *FASEB J.* 9, 726-735

Stepanova, A. N., & Alonso, J. M. (2005) Arabidopsis Ethylene Signaling Pathway. *Sci STKE* 276**,** cm3& cm4.

Ton, J., De Vos, M., Robben, C., Buchala, A., Metraux, J., Van Loon, L. & Pieterse, C. (2002) Characterization of *Arabidopsis* enhanced disease susceptibility mutants that are affected in systemically induced resistance. *Plant J.* 29**,** 11-21.

Von Dassow, G., Meir, E., Munro, E. & Odell, G. (2000) The segment polarity network is a robust developmental module. *Nature* 406, 188 – 192.

Yamada, S., Taketomi, T. & Yoshimura, A. (2004) Model analysis of difference between EGF pathway and FGF pathway. *Biochem. Biophys. Res. Commun.* 314, 1113–1120.